Crystal structures and magnetic properties of magnetically frustrated systems $BaLn_2O_4$ and $Ba_3Ln_4O_9$ (Ln = lanthanide)

2006 J. Phys.: Condens. Matter 18 333

(http://iopscience.iop.org/0953-8984/18/1/024)

INSTITUTE OF PHYSICS PUBLISHING JOURNAL OF PHYSICS: CONDENSED MATTER

J. Phys.: Condens. Matter **18** (2006) 333–344 doi:10.1088/0953-8984/18/1/024

Crystal structures and magnetic properties of magnetically frustrated systems $BaLn_2O_4$ and $Ba_3Ln_4O_9$ (Ln = lanthanide)

Yoshihiro Doi, Wataru Nakamori and Yukio Hinatsu

Division of Chemistry, Graduate School of Science, Hokkaido University, Sapporo 060-0810, Japan

E-mail: doi@sci.hokudai.ac.jp

Received 5 September 2005
Published 9 December 2005
Online at stacks.iop.org/JPhysCM/18/333

Abstract

The crystal structures and magnetic properties of the ternary oxides $BaLn_2O_4$ (Ln = Pr, Nd, Sm–Ho) and $Ba_3Ln_4O_9$ (Ln = Dy–Lu) have been investigated. These two series of compounds have the $CaFe_2O_4$-type structure with space group *Pnma* and a perovskite-related structure with space group *R*3, respectively. In both structures, the Ln ions locally adopt a triangle-based array, which has the possibility of resulting in a geometrically frustrated magnet. From the magnetic susceptibility measurements, it was found that some compounds show a magnetic anomaly at 2.2–4.0 K and the others are paramagnetic down to 1.8 K. The results of the specific heat measurements show that these compounds show a long-range antiferromagnetic ordering of Ln ions at 1.7 K (for $BaNd_2O_4$), 2.6 K ($BaGd_2O_4$), 0.8 K ($BaHo_2O_4$), and 4.0 K ($Ba_3Er_4O_9$).

1. Introduction

Oxides containing lanthanide (Ln) ions have been attracting interest since they often show anomalous magnetic properties derived from the unpaired 4f electrons at low temperatures. If the Ln ions adopt triangular geometric arrangements (triangular, Kagomé, pyrochlore, and fcc lattices) and if there exists an antiferromagnetic interaction between the nearest-neighbour Ln ions, they can show magnetic frustration. Geometrical frustration in magnetic materials is one of the most vigorous research fields in condensed matter science [1, 2]. Amongst such materials, the pyrochlore oxides $Ln_2M_2O_7$ (M = Ti, Sn, etc) are extensively studied. They have a lattice consisting of corner-shared Ln_4 tetrahedra, and some of them (Ln = Dy and Ho; M = Ti and Sn) show a phenomenon called 'spin ice' [3–5].

In order to explore new interesting materials, the research is now spreading to compounds with more complicated lattices. Recently, Karunadasa *et al* reported the results of magnetic

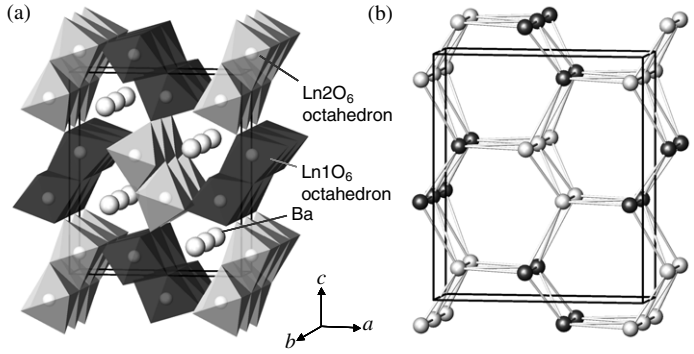

Figure 1. (a) The crystal structure of $BaLn_2O_4$ and (b) the framework of the Ln ions (black: Ln1; white: Ln2).

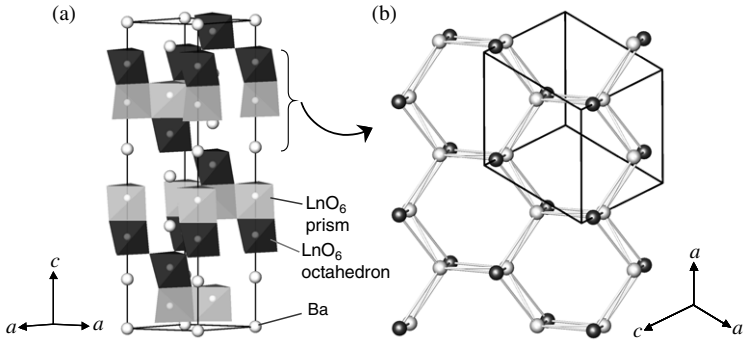

Figure 2. (a) The crystal structure of $Ba_3Ln_4O_9$ and (b) the framework of the Ln ions (black: Ln2 and Ln4; white: Ln1 and Ln3).

susceptibility and neutron diffraction measurements for $SrLn_2O_4$ (Ln = Gd, Dy–Yb) [6]. These compounds have a crystal structure with a triangle-based array of Ln ions: the honeycomb-like structure formed by zigzag chains consisting of edge-shared Ln_3 triangles. They show complicated magnetic properties, and magnetic anomalies were observed below 4 K, indicating the onset of a magnetic transition.

Here, we focused our attention on the magnetic properties of $BaLn_2O_4$ and $Ba_3Ln_4O_9$ in the $BaO–Ln_2O_3$ systems [7, 8]. Their syntheses and crystal structures have been reported by many researchers: $BaLn_2O_4$ for Ln = La, Pr, Nd, Sm–Er [7, 9–12] are isotypic with $SrLn_2O_4$, and $Ba_3Ln_4O_9$ for Ln = Sm–Lu [7, 13–17] have a perovskite-related structure. Their schematic structures are shown in figures 1 and 2. In $BaLn_2O_4$, all the Ln ions adopt the triangle-based array. On the other hand, the $Ba_3Ln_4O_9$ compounds have a trigonal symmetry, and the Ln ions occupy the octahedral and prismatic sites. The octahedra and prisms are connected by face-sharing, and they form Ln_2O_9 units. These units are linked by corner- and edge-sharing, and they locally make a triangle-based framework, which is similar to that observed in $BaLn_2O_4$. Therefore, it is expected that these two series of compounds may show anomalous magnetic properties reflecting the geometrical frustration. Detailed magnetic properties of these compounds at low temperatures have not been investigated except for the Pr compound [18]. In order to elucidate their basic magnetic properties, we report the syntheses, crystal structures, and results of the magnetic susceptibility and specific heat measurements.

Table 1. Structural parameters for $BaHo_2O_4$. (Note: space group *Pnma*; $a = 10.3946(2)$ Å, $b = 3.4517(1)$ Å, $c = 12.1100(3)$ Å, $R_{wp} = 8.70\%$, $R_p = 6.38\%$, $R_I = 1.61\%$, $R_e = 7.32\%$.)

Atom	Site	x	y	z	B (Å^2)
Ba	4c	0.7530(2)	1/4	0.6494(1)	0.49(3)
Ho1	4c	0.4220(2)	1/4	0.1091(1)	0.40(4)
Ho2	4c	0.4259(2)	1/4	0.6111(1)	0.53(4)
O1	4c	0.2120(10)	1/4	0.1554(11)	0.9(1)
O2	4c	0.1159(10)	1/4	0.4800(11)	0.9
O3	4c	0.5159(14)	1/4	0.7798(10)	0.9
O4	4c	0.4270(12)	1/4	0.4257(9)	0.9

2. Experimental details

Polycrystalline samples ($BaLn_2O_4$ and $Ba_3Ln_4O_9$) were prepared by solid-state reaction. As starting materials, $BaCO_3$, Ln_2O_3 (Ln = La, Nd, Sm–Gd, Dy–Lu), CeO_2, Pr_6O_{11}, Tb_4O_7 were used. Before use, La_2O_3 and Nd_2O_3 were dried at 1173 K overnight. For compounds of $BaLa_2O_4$, $BaPr_2O_4$, $Ba_3Eu_4O_9$, and $Ba_3Gd_4O_9$, 10% excess $BaCO_3$ was added because of the evaporation of barium. They were mixed in an agate mortar, and the mixtures were pressed into pellets and then heated in flowing Ar or H_2 atmosphere at 1423–1573 K for 1–8 h ($BaLn_2O_4$), or in air at 1573–1773 K for 3–12 h ($Ba_3Ln_4O_9$).

The x-ray diffraction measurements were performed at room temperature in the range $10° \leqslant 2\theta \leqslant 120°$ using a 2θ step size of 0.02° with Cu Kα radiation on a Rigaku MultiFlex diffractometer. In order to prevent sample decomposition by water and carbon dioxide in the air, all the measurements were carried out in an argon gas atmosphere. The x-ray diffraction data were analysed by the Rietveld technique, using the program RIETAN2000 [19].

The temperature dependence of the magnetic susceptibilities was measured under both zero-field-cooled (ZFC) and field-cooled (FC) conditions in an applied field of 0.1 T over the temperature range 1.8–300 K using a SQUID magnetometer (Quantum Design, MPMS-5S). For samples showing a magnetic anomaly above 1.8 K, specific heat measurements were performed using a relaxation technique with a commercial physical property measurement system (Quantum Design, PPMS model) in the temperature range 0.5–15 K (or 1.8–300 K). A sintered sample in the form of a pellet was mounted on a thin alumina plate with grease for better thermal contact.

3. Results and discussion

3.1. Sample preparation and crystal structure of $BaLn_2O_4$

$BaLn_2O_4$ compounds with Ln = Pr, Nd, Sm–Ho were successfully prepared in this study. On the other hand, the single phase for Ln = La, Ce, Er–Lu compounds could not be obtained because of the significant evaporation of barium (for Ln = La), no existence of the target phase (Ce), or the prior generation of $Ba_3Ln_4O_9$ phase (Er–Lu). The x-ray diffraction profile for $BaHo_2O_4$ is shown in figure 3(a). All the diffraction data for products obtained successfully were analysed by the Rietveld method. The refined lattice parameters are plotted against the ionic radius of Ln^{3+} in figure 4; they are in good agreement with the previous results [7, 9–12]. The structural parameters for $BaHo_2O_4$ are summarized in table 1.

The bond valence sums (BVSs) for Ln and Ba ions were calculated using the refined structural parameters, and they are plotted against the ionic Ln^{3+} radius in figure 5. The values

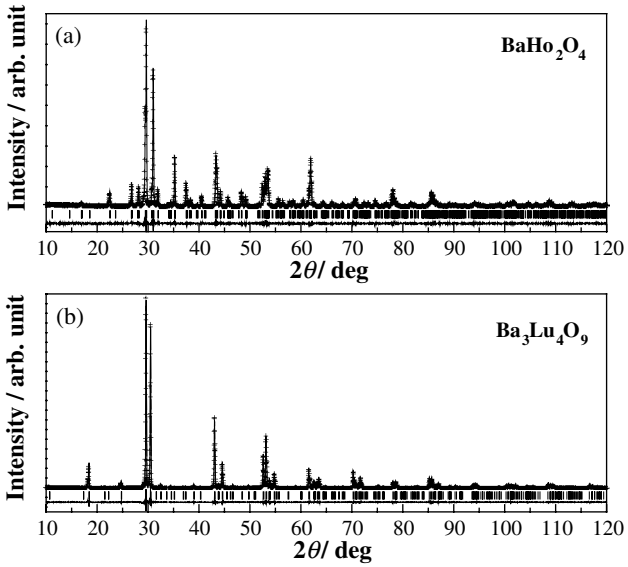

Figure 3. The x-ray diffraction profiles for (a) $BaHo_2O_4$ and (b) $Ba_3Lu_4O_9$.

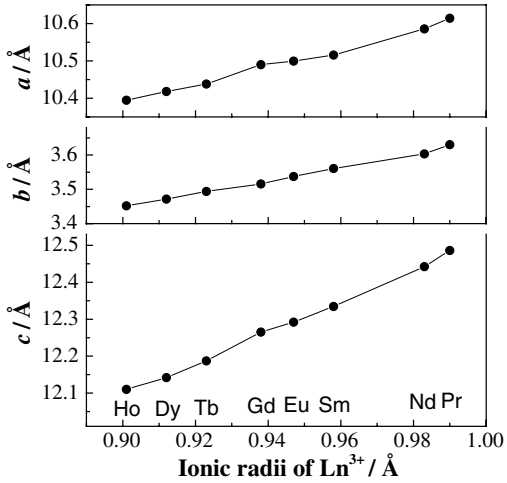

Figure 4. Variation of lattice parameters for $BaLn_2O_4$ against the ionic radius of Ln^{3+}.

for the Ln ion are almost constant (2.8–3.0) and reasonable for trivalent ions. Those for the Ba ion are close to 2.0 for Ln = Dy and Ho compounds; however, they are decreasing with increasing the ionic radius of Ln^{3+}. In this structure, Ba ions occupy the sites in the hexagonal tunnel formed by the honeycomb-like linkage of LnO_6 octahedra. As Wong-Ng *et al* pointed out previously for $BaNd_2O_4$ [11], this tunnel may be relatively large for the Ba ion in $BaLn_2O_4$ when the Ln^{3+} is large in size. For smaller Ln (=Er–Lu) ions, the BVS values probably exceed 2. This accounts for the difficulty in preparing compounds with smaller Ln ions, i.e., the size of the tunnel becomes too small to locate the Ba ion.

Figure 6(a) shows the framework of Ln ions in $BaLn_2O_4$, and the Ln–Ln interatomic distances for the case of Ln = Ho. For all the $BaLn_2O_4$ compounds, the Ln1–Ln1 and Ln2–

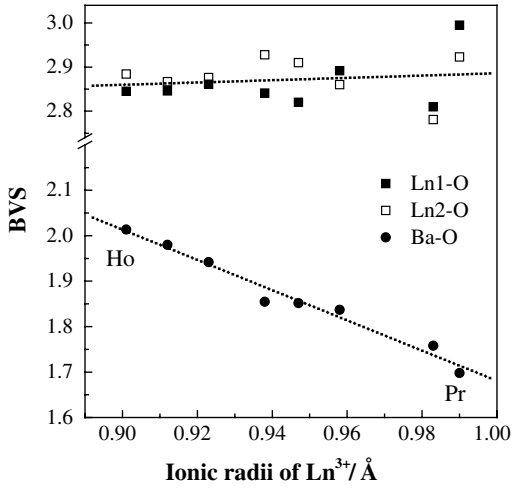

Figure 5. Variation of the bond valence sum of Ba and Ln ions in $BaLn_2O_4$ against the ionic radius of Ln^{3+}.

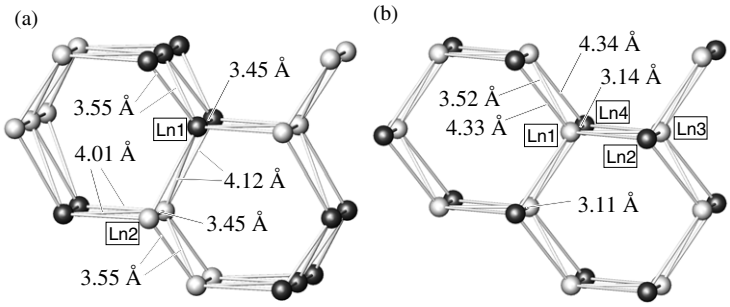

Figure 6. Interatomic distances of Ln ions in (a) $BaHo_2O_4$ and (b) $Ba_3Lu_4O_9$.

Ln2 distances are in the range 3.45–3.74 Å, and the Ln1–Ln2 distances are 4.01–4.24 Å; the ratio of the maximum and minimum distances is ∼1.2. These structural features are in good agreement with those for the $SrLn_2O_4$ series [6]. In these structures, all of the Ln ions form triangles, and in particular, those consisting of only Ln1 (or Ln2) ions are approximately regular in shape. Thus, the magnetic interaction between Ln ions is expected to be frustrated.

3.2. Sample preparation and crystal structure of $Ba_3Ln_4O_9$

The $Ba_3Ln_4O_9$ compounds for Ln = Dy–Lu were crystallized in a single phase. For Ln = Eu and Gd, the products contained some amounts of $BaLn_2O_4$ and Ln_2O_3 (∼10%) as impurity phases, and for La–Nd, Sm, and Tb, the target phase could not be detected. Figure 3(b) shows the x-ray diffraction profile for $Ba_3Lu_4O_9$. The data for Ln = Dy–Lu compounds were analysed by the Rietveld method, and the structural parameters determined for $Ba_3Lu_4O_9$ are listed in table 2. The lattice parameters are plotted against the ionic radius of Ln^{3+} in figure 7, and they are in good agreement with the previous results [7, 13–17].

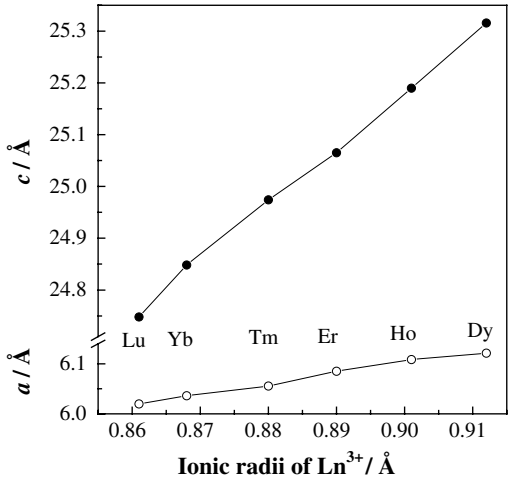

Figure 7. Variation of lattice parameters for $Ba_3Ln_4O_9$ against the ionic radius of Ln^{3+}.

Table 2. Structural parameters for $Ba_3Lu_4O_9$. (Note: space group $R3$; $a = 6.0200(2)$ Å, $c = 24.7481(5)$ Å, $R_{wp} = 10.39\%$, $R_p = 7.51\%$, $R_I = 1.81\%$, $R_e = 6.70\%$.)

Atom	Site	x	y	z	B (Å^2)
Ba1	3a	0	0	0[a]	1.0(1)
Ba2	3a	0	0	0.1614(2)	1.0
Ba3	3a	0	0	0.5859(4)	1.0
Lu1	3a	0	0	0.4262(4)	0.9(1)
Lu2	3a	0	0	0.8638(5)	0.9
Lu3	3a	0	0	0.7380(4)	0.9
Lu4	3a	0	0	0.2994(6)	0.9
O1	9b	0.791(7)	0.664(8)	0.244(1)	1.0(4)
O2	9b	−0.006(6)	0.436(7)	0.135(1)	1.0
O3	9b	0.022(8)	0.405(6)	0.219(1)	1.0

[a] Fixed to 0.

The schematic crystal structure of $Ba_3Ln_4O_9$ is illustrated in figure 2. This structure can be regarded as one of the perovskite-derived structures. The structure of a normal perovskite ABO_3 consists of the $[AO_3]$ layers stacking in the cubic closed-packed manner and B ions filling the space (octahedral sites) between layers. In the case of the B-ion-rich perovskite $Ba_3Ln_4O_9$, half of the Ln ions (Ln2 and Ln4) occupy the normal octahedral sites, while the rest (Ln1 and Ln3) occupy distorted prismatic sites. The Ln ions in the latter fill the space between $[BaO_3]$ layers twice as densely as those in the former, and the octahedra and prisms share faces, forming the Ln_2O_9 units. This may explain the experimental results that $Ba_3Ln_4O_9$ with larger Ln ions were not formed.

Figure 6(b) shows the framework of Ln ions in the $Ba_3Ln_4O_9$ compounds. The interatomic distances between Ln ions are calculated from the refined structural parameters for all the $Ba_3Ln_4O_9$ compounds. Among them, the Ln–Ln distances in the Ln_2O_9 unit (the face-sharing LnO_6 octahedron and LnO_6 prism) is the shortest: 3.11–3.32 Å (Ln1–Ln4) and 3.12–3.27 Å (Ln2–Ln3). The Ln–Ln distance for the edge-sharing LnO_6 prisms is 3.52–3.61 Å (Ln1–Ln3) and those for the corner-sharing LnO_6 octahedra are 4.24–4.39 Å (Ln1–Ln2), 4.24–4.38 Å (Ln3–Ln4), and 4.30–4.38 Å (Ln2–Ln4). Here, it should be noted that there is a difference

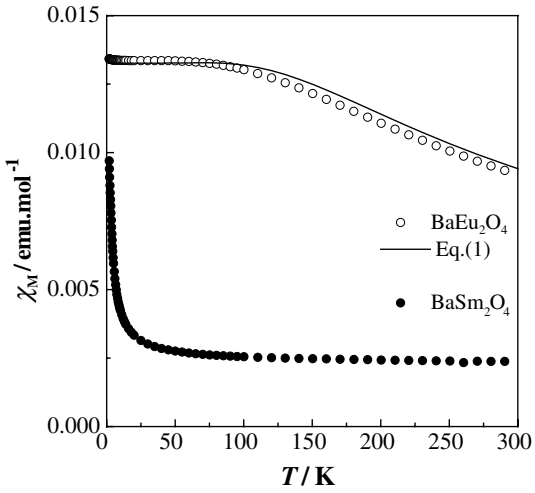

Figure 8. Temperature dependence of the magnetic susceptibilities for $BaSm_2O_4$ and $BaEu_2O_4$. The solid curve is the magnetic susceptibility calculated for $BaEu_2O_4$ by equation (1) (see text).

in the structures between $BaLn_2O_4$ and $Ba_3Ln_4O_9$. The honeycomb-like array of the former (figure 1(b)) stacks directly along the *b*-axis, keeping its tunnel structure, and that of the latter (figure 2(b)) stacks obliquely along the *c*-axis with translational symmetry (2/3, 1/3, 1/3)+ and (1/3, 2/3, 2/3)+ in space group *R*3. This difference in the way of stacking the framework and the larger ratio of the maximum and minimum Ln–Ln distances in the $Ba_3Ln_4O_9$ (∼1.4) than that in the $BaLn_2O_4$ (∼1.2) would make the frustration in $Ba_3Ln_4O_9$ weaker. Frustrated behaviour may also be expected in $Ba_3Ln_4O_9$ due to the triangular array of Ln ions.

3.3. Magnetic properties of $BaLn_2O_4$

From the magnetic susceptibility measurements for $BaLn_2O_4$ (Ln = Pr, Nd, Gd–Ho), it is found that the Pr, Tb and Dy compounds are paramagnetic down to 1.8 K, while the Nd, Gd, and Ho compounds show a magnetic anomaly at 2.2–3.6 K (also see figures 9(a)–11(a)). They show Curie–Weiss-like behaviour at higher temperatures. Their effective magnetic moments and Weiss constants are determined by the Curie–Weiss law using the data between 150 and 300 K, and they are listed in table 3. The effective magnetic moments are very close to the calculated moments of free Ln^{3+} ions. The negative Weiss constants indicate that the predominant magnetic interaction between Ln^{3+} ions is antiferromagnetic.

The magnetic susceptibilities for $BaSm_2O_4$ and $BaEu_2O_4$ are plotted as a function of temperature in figure 8. No magnetic transition was observed down to 1.8 K. Both sets of data do not obey the Curie–Weiss law. For the Sm^{3+} and Eu^{3+} ions, the multiplet levels are not large compared to k_BT (k_B: Boltzmann constant), so the excited states should contribute to the magnetic susceptibility. A susceptibility plateau of $BaEu_2O_4$ is observed below 80 K, which is attributed to the temperature-independent term of the Van Vleck formula. Considering the contribution of excited states ^7F_J ($J = 1, 2, \ldots, 6$), the magnetic susceptibility of $BaEu_2O_4$ was fitted by using the following equation [20]:

$$\chi(Eu^{3+}) = \frac{N_A\mu_B^2}{3k_B\gamma T}\frac{24 + (13.5\gamma - 1.5)e^{-\gamma} + (67.5\gamma - 2.5)e^{-3\gamma} + (189\gamma - 3.5)e^{-6\gamma} + \cdots}{1 + 3e^{-\gamma} + 5e^{-3\gamma} + 7e^{-6\gamma} + \cdots}, \quad (1)$$

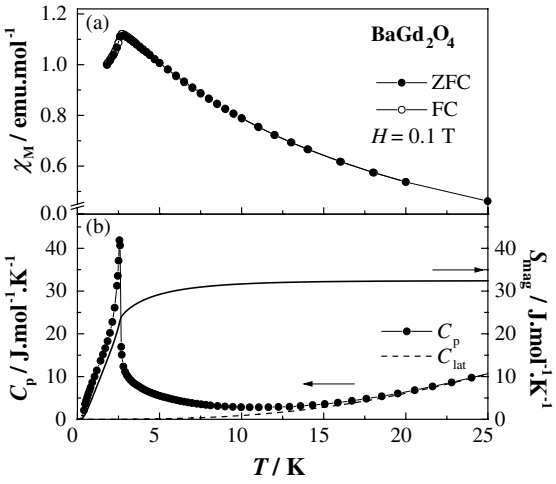

Figure 9. Temperature dependence of (a) the magnetic susceptibility, (b) specific heat and magnetic entropy of $BaGd_2O_4$.

Table 3. The effective magnetic moments (μ_{eff}: experimental, μ_{cal}: calculated) per Ln ion, Weiss constant, and Néel temperature for $BaLn_2O_4$.

Compound	μ_{eff}/μ_B	μ_{cal}/μ_B	θ (K)	θ_{LT}[c] (K)	T_N (K)
$BaPr_2O_4$	3.66(1)	3.58	−109.7(13)	—	—
$BaNd_2O_4$	3.57(1)	3.62	−42.3(7)	−6.5(2)	1.7
$BaSm_2O_4$	1.69[a]	1.55[b]	—	−16(1)	<1.8
$BaEu_2O_4$	3.41[a]	3.40[b]	—	—	—
$BaGd_2O_4$	7.96(1)	7.94	−8.6(2)	−11.9(1)	2.6
$BaTb_2O_4$	9.72(1)	9.72	−21.1(2)	−20.2(5)	<1.8
$BaDy_2O_4$	10.81(1)	10.63	−23.0(5)	−15.7(4)	<1.8
$BaHo_2O_4$	10.42(1)	10.58	−12.7(1)	−10.1(2)	0.8

[a] Observed values at room temperature.
[b] Calculated values by Van Vleck [20].
[c] Weiss constants obtained from low-temperature (5–20 K) data.

where N_A is Avogadro's number and $\gamma = \lambda/k_BT$ is 1/21 of the ratio of the overall multiplet width to k_BT. By fitting this equation to the experimental magnetic susceptibility, the spin–orbit coupling constant λ was obtained to be 314(2) cm^{-1}. This value is reasonable compared with those reported in other oxides, for example, 327 cm^{-1} ($LiEuO_2$) [21] and 347 cm^{-1} ($NaEuO_2$) [22].

Figure 9(a) shows the detailed temperature dependence of the magnetic susceptibility for $BaGd_2O_4$ in lower temperature region. A cusp, suggesting the occurrence of an antiferromagnetic transition, is observed at 2.6 K (the Néel temperature, T_N). To further investigate this magnetic anomaly, a specific heat (C_p) measurement was performed, and the result is shown in figure 9(b). The data show a λ-type anomaly at the same temperature, which indicates that a long-range antiferromagnetic ordering of Gd^{3+} ions occurs at this temperature. The specific heat mainly consists of the lattice (C_{lat}) and magnetic (C_{mag}) contributions around this experimental temperature range. To obtain the magnetic contribution, the lattice contribution is estimated by fitting a polynomial function of temperature, $C_{lat} = aT^3 + bT^5 + cT^7$, to the data between 25 and 45 K. The temperature dependence of the

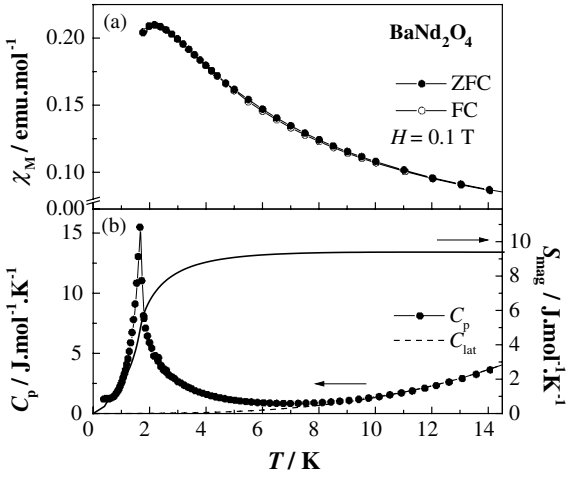

Figure 10. Temperature dependence of (a) the magnetic susceptibility, (b) specific heat and magnetic entropy for $BaNd_2O_4$.

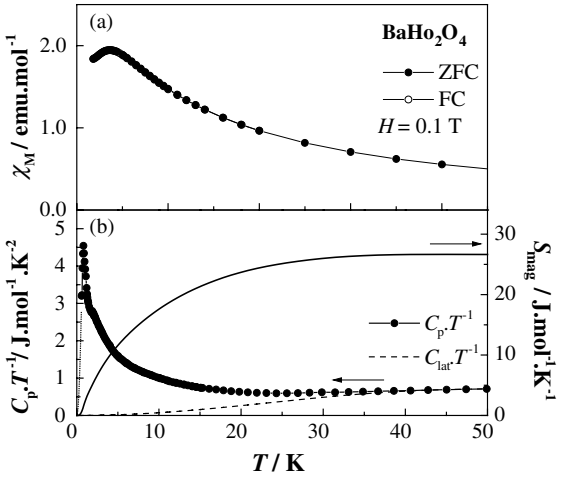

Figure 11. Temperature dependence of (a) the magnetic susceptibility, (b) specific heat and magnetic entropy for $BaHo_2O_4$.

magnetic entropy, calculated from $S_{mag} = \int (C_{mag}/T)\,dT$, is plotted as a solid curve in figure 9(b). The magnetic entropy change (ΔS_{mag}) associated with the antiferromagnetic transition is determined to be 16.3 J mol^{-1} K^{-1} per Gd ion (because there are two Gd^{3+} ions per formula unit). This value is in good agreement with that expected from the eightfold-degenerate ground state of $4f^7$ ion, $R\ln(2S+1) = R\ln 8 = 17.32$ J mol^{-1} K^{-1}.

The magnetic susceptibility and specific heat for $BaNd_2O_4$ at low temperatures are plotted in figure 10. The specific heat shows a λ-type anomaly at 1.7 K, which indicates the occurrence of long-range magnetic ordering. A broad peak around 2.2 K observed in the magnetic susceptibility may be due to the onset of the antiferromagnetic transition. The magnetic entropy is calculated in the same way as the case for $BaGd_2O_4$, and is shown as a solid line in figure 10(b). The value of ΔS_{mag} is determined to be 4.7 J mol^{-1} K^{-1} per Nd ion. This value is

close to not $R\ln(2J+1) = R\ln 10 = 19.14\,\mathrm{J\,mol^{-1}\,K^{-1}}$ but $R\ln 2 = 5.76\,\mathrm{J\,mol^{-1}\,K^{-1}}$. The ground multiplet $^4I_{9/2}$ of Nd^{3+} should be split into five Kramers' doublets in a low symmetric crystal-field; the observed magnetic entropy of $R\ln 2$ indicates that the ground doublet is selectively populated at low temperatures and this state causes the antiferromagnetic transition.

Figure 11 shows the temperature dependence of the magnetic susceptibility, specific heat divided by temperature, and magnetic entropy for $BaHo_2O_4$. This compound shows a broad anomaly around 3.6 K in the magnetic susceptibility, and from the specific heat, it is found that the actual antiferromagnetic transition occurs at 0.8 K. At higher temperatures, the magnetic entropy reaches 13.3 $\mathrm{J\,mol^{-1}\,K^{-1}}$ per Ho ion. This value is comparable with $R\ln 5 = 13.38\,\mathrm{J\,mol^{-1}\,K^{-1}}$ or $R\ln 6 = 14.90\,\mathrm{J\,mol^{-1}\,K^{-1}}$. This result indicates that the ground multiplet $^5I_8$ of Ho^{3+} is split into many states by the crystal-field and the ground and some low-lying excited states (the total degeneracy is 5 or 6) are populated at low temperatures. In a regular octahedral crystal-field, the ground state is a Γ_3 (doublet) or Γ_1 (singlet), and a low-lying Γ_4 (triplet) state exists [23]. At $T_N = 0.8$ K, the magnetic entropy is only $0.7\,\mathrm{J\,mol^{-1}\,K^{-1}}$, and it shows a continuous increasing up to ~38 K. According to the previous neutron diffraction measurement for $SrHo_2O_4$ [6], some broad magnetic reflections below ~40 K and the rapid increasing of their intensities below ~4 K were observed. They were explained as a crossover phenomenon from short-range (T = 4–40 K) to two-dimensional (in the honeycomb layer) long-range ordering ($T < 4$ K). Thus, our results for $BaHo_2O_4$ can be understood by the following way: short-range magnetic ordering below ~38 K, two-dimensional ordering at 3.6 K, and final three-dimensional ordering at 0.8 K.

The $BaLn_2O_4$ compounds have a triangle-based array of Ln^{3+} ions and are expected to behave as frustrated magnets. Geometrically frustrated materials often show a large ratio $|\theta|/T_N$ since such a frustration suppresses the long-range magnetic ordering [1]. The Weiss constant in a low-temperature region, θ_{LT}, (table 3) was also calculated to prevent its overestimation by the slight convexity of the χ^{-1} versus T curve due to the crystal-field effect. In the case of $BaLn_2O_4$, the $|\theta_{LT}|/T_N$ values are relatively large: 3.8 (for Ln = Nd) and 4.6 (Gd), 12.6 (Ho), and >8 (Sm, Tb, Dy). In addition, it is found that they show the different magnetic behaviour around T_N, i.e., a typical three-dimensional antiferromagnetic ordering is observed for $BaGd_2O_4$ while a broad susceptibility peak is observed above T_N in the χ versus T curves for $BaNd_2O_4$ and $BaHo_2O_4$. In particular, $BaHo_2O_4$ shows the possibility of gradual ordering of Ho^{3+} moments, and its T_N (0.8 K) is much lower than the onset temperature of short-range ordering (~38 K). There results indicate that the magnetic ordering is highly suppressed by the magnetic frustration.

3.4. Magnetic properties of $Ba_3Ln_4O_9$

Magnetic susceptibility measurements for $Ba_3Ln_4O_9$ (Ln = Dy–Yb) show that only $Ba_3Er_4O_9$ exhibits a magnetic anomaly at 4.0 K while the others are paramagnetic down to 1.8 K. The effective magnetic moments and Weiss constants determined by the Curie–Weiss fitting (T = 150–300 K) are listed in table 4. The effective magnetic moments are in good agreement with those for the free Ln^{3+} ion. The negative Weiss constants show the existence of antiferromagnetic interaction between Ln ions.

The temperature dependences of the magnetic susceptibility and specific heat for $Ba_3Er_4O_9$ at low temperatures are plotted in figure 12. Both curves show an anomaly at 4.0 K, indicating the antiferromagnetic transition. The S_{mag}–T curve is calculated from the specific heat data in the same way as the case for $BaGd_2O_4$, and is shown as a solid curve in figure 12(b). The magnetic entropy change is estimated to be $5.17\,\mathrm{J\,mol^{-1}\,K^{-1}}$ per Er ion, which is close to $R\ln 2 = 5.76\,\mathrm{J\,mol^{-1}\,K^{-1}}$. Considering that the Er^{3+} is a Kramers' ion, this result indicates

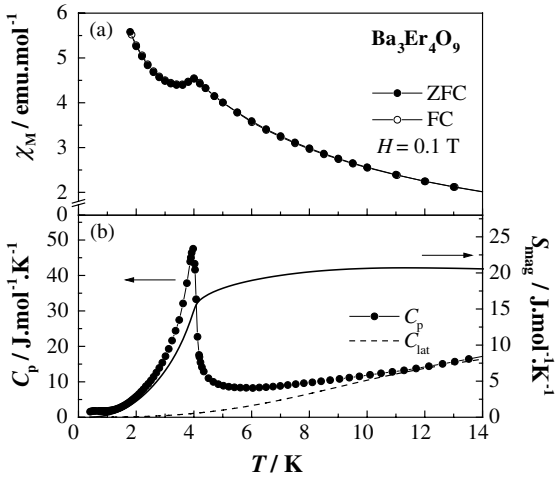

Figure 12. Temperature dependence of (a) the magnetic susceptibility, (b) specific heat and magnetic entropy for $Ba_3Er_4O_9$.

Table 4. The effective magnetic moments (μ_{eff}: observed, μ_{cal}: calculated) per Ln ion, Weiss constant, and Néel temperature for $Ba_3Ln_4O_9$.

Compound	μ_{eff}/μ_B	μ_{cal}/μ_B	θ (K)	θ_{LT}[a] (K)	T_N (K)
$Ba_3Dy_4O_9$	10.67(1)	10.63	−13.2(3)	−4.9(1)	<1.8
$Ba_3Ho_4O_9$	10.37(1)	10.58	−10.9(2)	−3.4(1)	<1.8
$Ba_3Er_4O_9$	9.32(1)	9.59	−7.9(3)	−4.5(1)	4.0
$Ba_3Tm_4O_9$	7.12(1)	7.55	−19.0(3)	−6.5(3)	<1.8
$Ba_3Yb_4O_9$	4.63(1)	4.54	−80.0(13)	−5.0(1)	<1.8

[a] Weiss constants determined in the lower-temperature region (5–20 K).

that both Er^{3+} ions in octahedral and prismatic sites have the doublet ground states. The magnetic entropy reaches 70% (3.7 J mol^{-1} K^{-1}) of the observed ΔS_{mag} at T_N and the $|\theta_{LT}|/T_N$ is near to the unity (∼1.1); clear evidence for the frustration is not found in this compound.

4. Summary

The crystal structures and magnetic properties of $BaLn_2O_4$ and $Ba_3Ln_4O_9$, in which the Ln ions adopt a triangle-based array, have been studied. The $BaLn_2O_4$ compounds with Ln = Nd, Gd, and Ho show an anomaly in the magnetic susceptibility at 2.2–3.6 K. From the specific heat measurements, it is found that the actual antiferromagnetic transition occurs at 1.7, 2.6, and 0.8 K, respectively. In particular, $BaHo_2O_4$ shows the gradual ordering of Ho^{3+} moments with decreasing temperature, indicating a high suppression of magnetic ordering. In addition, relatively high $|\theta_{LT}|/T_N$ values (3.8–12.6) of the $BaLn_2O_4$ compounds suggest the possibility of geometrical magnetic frustration due to the triangular motif formed by the Ln ions. In the $Ba_3Ln_4O_9$ compounds, only $Ba_3Er_4O_9$ shows an antiferromagnetic transition (T_N = 4.0 K) while the others are paramagnetic down to 1.8 K. Their crystal structures locally have a triangle-based array of Ln ions similar to that of $BaLn_2O_4$; however, no feature of a frustrated magnet was observed in $Ba_3Er_4O_9$. For the $Ba_3Ln_4O_9$ compounds with Ln = Dy Ho, Tm, and Yb, the possibility of magnetic frustration still remains because the $|\theta_{LT}|/T_N$ values may be large; thus, further measurements will be carried out to clarify this point.

Acknowledgments

This research was partially supported by the Ministry of Education, Culture, Sports, Science and Technology, Japan, a Grant-in-Aid for Young Scientists (No. 16750043) and Scientific Research Priority Area 'Panoscopic Assembling and High Ordered Functions for Rare Earth Materials' (No. 17042003).

References

[1] Greedan J E 2001 *J. Mater. Chem.* **11** 37–53
[2] Ramirez A P 1994 *Annu. Rev. Mater. Sci.* **24** 453–80
[3] Ramirez A P, Hayashi A, Cava R J, Siddharthan R and Shastry B S 1999 *Nature* **9** 333–5
[4] Matsuhira K, Hinatsu Y, Tenya K and Sakakibara T 2000 *J. Phys.: Condens. Matter* **12** L649–56
[5] Matsuhira K, Hinatsu Y, Tenya K, Amitsuka H and Sakakibara T 2002 *J. Phys. Soc. Japan* **71** 1576–82
[6] Karunadasa H, Huang Q, Ueland B G, Lynn J W, Schiffer P, Regan K A and Cava R J 2005 *Phys. Rev.* B **71** 144414
[7] Lopato L M 1976 *Ceram. Int.* **2** 18–32
[8] Hodorowics E, Hodorowics S A and Eick H A 1990 *J. Solid State Chem.* **84** 401–7
[9] Wong-Ng W and Paretzkin B 1991 *Powder Diffr.* **6** 187–9
[10] Cascales C and Rasines I 1995 *Powder Diffr.* **10** 122–6
[11] Wong-Ng W, Cook L P, Suh J, Coutts R, Stalick J K, Levin I and Huang Q 2003 *J. Solid State Chem.* **173** 476–88
[12] Mitamura T, Ogino H, Kobayashi H, Mori T and Yamamura H 1993 *J. Am. Ceram. Soc.* **76** 2127–8
[13] Brauer G and Kristen H 1980 *Z. Anorg. Allg. Chem.* **462** 35–41
[14] Krüger J and Müller-Buschbaum Hk 1983 *Z. Anorg. Allg. Chem.* **512** 59–64
[15] Krueger J and Mueller-Buschbaum Hk 1983 *Rev. Chim. Miner.* **20** 456–61
[16] Müller-Buschbaum Hk and Scheikowski M 1990 *Z. Anorg. Allg. Chem.* **591** 181–7
[17] Müller-Buschbaum Hk and Schrandt O 1993 *J. Alloys Compounds* **191** 151–4
[18] Felner I, Yeshurun Y, Hilscher G, Holubar T, Schaudy G, Yaron U, Cohen O, Wolfus Y, Yacoby E R, Klein L, Potter F H, Rastomjee C S and Egdell R G 1992 *Phys. Rev.* B **46** 9132–41
[19] Izumi F and Ikeda T 2000 *Mater. Sci. Forum* **321–324** 198–203
[20] Van Vleck J H 1932 *The Theory of Electric and Magnetic Susceptibilities* (Oxford: Clarendon)
[21] Hashimoto Y, Wakeshima W, Matsuhira K, Hinatsu Y and Ishii Y 2002 *Chem. Mater.* **14** 3245–51
[22] Hashimoto Y, Wakeshima W and Hinatsu Y 2003 *J. Solid State Chem.* **176** 266–72
[23] Lea K R, Leask M J M and Wolf W P 1962 *J. Phys. Chem. Solids* **23** 1381–405